Carbon Nanohorns and Their High Potential in Biological Applications

Minfang Zhang and Masako Yudasaka

Abstract Carbon nanohorns, also called single-wall carbon nanohorns (SWNHs), are single-graphene tubules with horn-shaped tips, and were first reported by Iijima and colleagues in 1999 [1]. The tubule lengths and diameters range from 30 to 50 nm and 2 to 5 nm, respectively, and therefore, SWNHs are not uniform in size. Thousands of SWNHs assemble to form an aggregate, which in turn has an average diameter of ~80–100 nm. SWNHs are produced in large quantities (1 kg/day) by laser ablation of graphite. This process does not require a metal catalyst, and thus it is possible to prepare SWNHs with high purity (>95 %). Owing to their large surface area, molecular sieving effects and photo-thermal conversion characteristics, SWNHs show promise for applications in gas adsorption and storage, biosensor and nanomedicine such as drug delivery and photo-hyperthermia cancer therapy. In this chapter, we briefly introduce nanohorn production methods, biomaterial properties, and functionalization, and then highlight the potential use of SWNHs in various biological research fields. Issues concerning toxicity and biodegradation are also discussed.

Keywords Biomaterial · Biosensor · Carbon nanohorn · Drug delivery system · Nanomedicine · Photo-hyperthermia

M. Zhang (✉)
Nanotube Application Research Center, National Institute of Advanced Industrial Science and Technology (AIST), Tsukuba, Japan
e-mail: m-zhang@aist.go.jp

M. Yudasaka
Nanomaterials Research Institute, National Institute of Advanced Industrial Science and Technology (AIST), Tsukuba, Japan
e-mail: m-yudasaka@aist.go.jp

M. Yudasaka
Meijo University, Nagoya, Japan

N. Yang et al. (eds.), *Carbon Nanoparticles and Nanostructures*,
Carbon Nanostructures, DOI 10.1007/978-3-319-28782-9_3

1 Introduction

Single-wall carbon nanohorns (SWNHs) were first reported in 1999 [1]. SWNHs have a single-graphene tubule structure, conferring unique characteristics to the biomaterial. The nanohorns are produced in large quantities at high purity without using metal catalysts. The superior pore structure of SWNHs (i.e., large surface area and an ample interior nanospace) suggests their prospective use in gas storage, catalyst support, and drug delivery applications. Moreover, like other carbon nanomaterials (e.g., single-walled carbon nanotubes (SWNTs) [2] and multiwall carbon nanotubes (MWNTs)) [3], SWNHs absorb light in a wide spectrum of wavelengths, ranging from infrared to ultraviolet. They also generate heat, which could be beneficial for their utilization as photo-hyperthermia agents in cancer therapy and as photo-thermal energy conversion devices for the regeneration of lost heat. In this chapter, we briefly introduce the production, biomaterial properties, and functionalization of SWNHs, and then focus on current and proposed applications of SWNHs in biological research fields.

1.1 SWNH Production

Two representative methods are currently employed for the production of SWNHs with high purity: carbon dioxide (CO_2) laser ablation and arc discharge. The size distribution and purity of the SWNHs can be changed by varying production parameters, such as temperature, pressure, and laser or arc power.

Laser ablation The earliest report [1] of SWNH fabrication by Iijima and colleagues [1] utilized a CO_2 laser ablation technique for the generation of carbon nanohorns at room temperature without a metal catalyst (Fig. 1). The SWNH generator employed in this study consisted of two parts: a high-power CO_2 laser source (wavelength = ~0.6 μm; maximum power = 5 kW) and a reaction chamber. Argon (Ar) gas was introduced into and flowed throughout the inner chamber

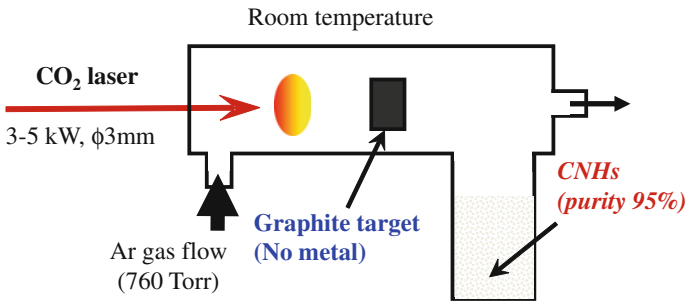

Fig. 1 Schematic diagram of SWNH production by laser ablation

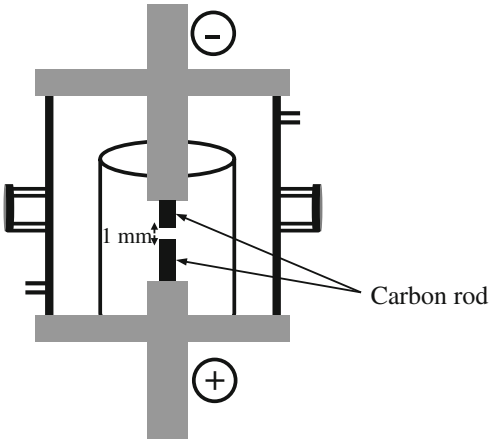

Fig. 2 Arc discharge device for SWNH production [6]

to carry the nanohorn products to the collection chamber under a pressure of 760 Torr at room temperature. The graphite target was placed in the middle of the reaction chamber and exposed to the laser beam [1, 4]. For large-scale production of SWNHs, the graphite target was replaced by a graphite rod, which was continuously rotated and moved along its axis so that a new surface was constantly exposed to the laser beam [5]. This setup resulted in a production rate of ~1 kg/day and a purity of the resultant as-grown SWNHs of ~95 % [5].

Arc discharge SWNHs are also prepared by direct current (DC) arc discharge [6–9]. DC arc discharge is carried out in a water-cooled stainless steel chamber [6] (Fig. 2). Two electrodes corresponding to pure carbon rods are separated from each other by a constant distance of ~1 mm. The arc discharge between the carbon rods is conducted under an atmospheric pressure of air [6, 7], nitrogen (N_2) [8, 9], water [10], CO_2, or carbon monoxide (CO) [7]. In the arc discharge system described in [6], the electric power density on the carbon rod surface was 9 kW/cm^2, and the SWNHs were deposited on the surface of the chamber. The mean size of the prepared SWNH particles was approximately 50 nm, which is smaller than that of the as-grown SWNHs prepared by CO_2 laser ablation. Pre-heating of the carbon rod to a temperature of up to 1000 °C before ignition of the arc improved the quality of manufactured SWNHs [6].

1.2 SWNH Properties

Structure The SWNH [1] is a single-graphene tubule of an irregular shape with non-uniform diameters of 2–5 nm, a length of 30–50 nm, and a horn-shaped tip (Fig. 3a). The tips often have cone angles of ~19° indicating the existence of five pentagonal rings. Thousands of SWNHs assemble to form a nanohorn aggregate,

which itself has an average diameter of ~80–100 nm (Fig. 3b, c). The distance between neighboring walls of the SWNH aggregate is approximately 0.4 nm [11], or larger than the basal plane distance of graphite (0.335 nm). Three different types of SWNH aggregates have been identified so far: the "dahlia-like" aggregate, the

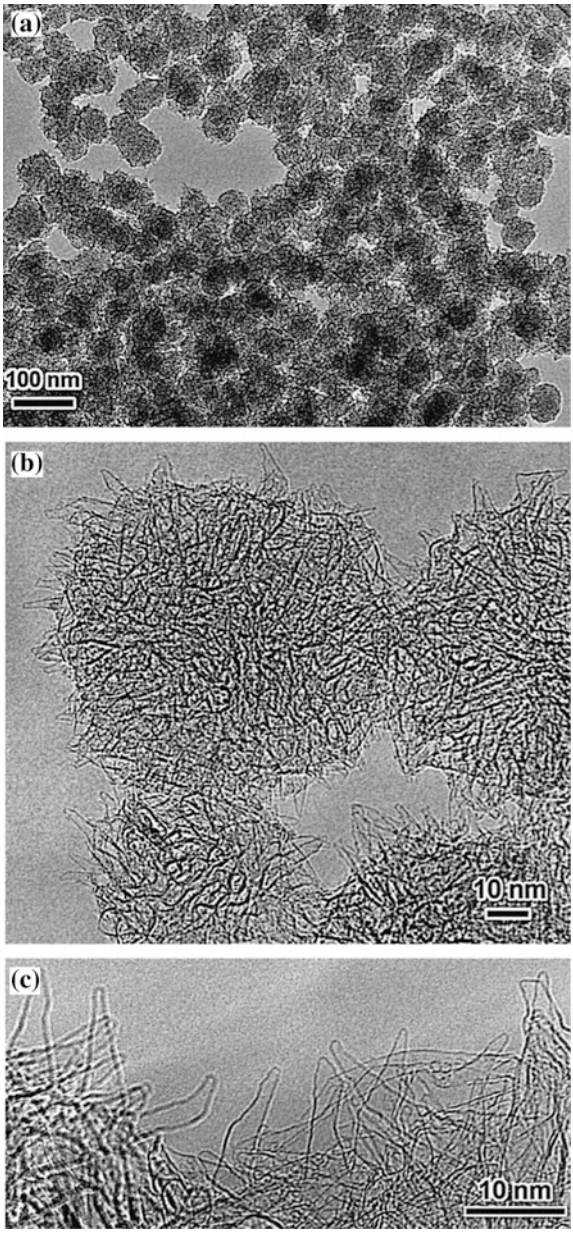

Fig. 3 **a** TEM image of SWNHs generated by CO_2 laser ablation. The SWNH product consists of spherical particles that are nearly uniform in size, with a diameter of 80 nm. **b** Magnified TEM image of SWNHs showing aggregations of individual tubule-like structures with protruding tips. **c** Highly magnified TEM image of the edge regions of the graphitic aggregate showing conical horn-like protrusions of ≤20 nm in length along the aggregate surface, with some modified shapes [1]

"bud-like" aggregate, and the "seed-like" aggregate [1]. In the first type of aggregate, SWNH tips protrude from the aggregate surface (Fig. 3b), while in the second and third types, the SWNHs appear to develop inside the aggregate itself. Different aggregate types are selectively produced by laser ablation with different gases. For example, "dahlia-like" SWNH aggregates are produced with a yield of 95 % when the buffer gas is Ar (760 Torr), while "bud-like" SWNH aggregates are formed with a yield of 70–80 % when either helium (He) or N_2 gas is employed at 760 Torr [12].

Porosity and hole-opening The pore structure of SWNHs has been extensively studied through simulation and adsorption experiments [13]. Isotherm measurements of N_2 adsorption at 77 K and high-pressure He buoyancy at 303 K reveal that as-grown SWNHs with closed tubules have a specific surface area of $\sim$300 m^2/g [14] and a total pore volume of $\sim$0.40 ml/g [15].

Nanoscale holes or windows can be generated on the tubule walls or tips by oxidation of SWNHs with oxygen (O_2) [16–19], CO_2 [20], or oxidative acids [15, 21, 22]. The number and size of the nanowindows so-generated are controlled by oxidation conditions [17]. Oxidation with a slow temperature increase of 1 °C/min in a low O_2 concentration (21 % in air) yields hole openings with little generation of carbonaceous dust [18]. After such oxidation-induced holes are created on the SWNH wall, the resultant nanohorn surface areas, total pore volume, and particle density are reportedly 1450–1460 m^2/g [15, 16], 1.05 ml/g [15], and 2.05 g/ml [17], respectively.

The SWNH possesses three adsorption sites: the inter-SWNH micropore, the interior wall surface, and the interior space; the volume ratio of the three is about 1:2:2 [17]. Approximately 11 and 36 % of the intraparticle pore spaces are opened by oxidation at 573 and 623 K, respectively. Treatment of SWNHs with nitric acid (HNO_3) induces the intercalation of HNO_3 into narrow interstitial spaces, further increasing pore volume through the development of microporosity [15]. The obtained ultra-microporous SWNH aggregates show a high storage capacity (100 mg/g) for methane [15].

Holes opened on the SWNH tubule walls are visible by high resolution transmission electron microscopy (TEM). Figure 4a shows holes generated by oxidation in O_2, and Fig. 4b shows the size distributions of the holes (0.5–1.0 nm at the tip, and 0.5–1.5 nm on the sidewalls) measured on the TEM images [19]. Therefore, materials of a size smaller than 1.5 nm, such as fullerenes, can be readily incorporated inside the SWNHs.

Holes or nanowindows introduced in the SWNH wall are differentially closed by high temperatures. Constant-temperature tight-binding molecular dynamic (TBMD) simulations indicate that holes in the sidewalls are not easily closed by thermal annealing, unlike those at the tips [23]. This finding provides an explanation for why some SWNH holes remain open following exposure to high temperatures [24]. A proposed hole-closing mechanism suggests that the holes at the tips undergo a closed-open-closed evolution when the initial hole size is >0.7–0.9 nm, while the same holes close rapidly and remain in that state when the initial hole sizes are ≤0.7–0.9 nm [24].

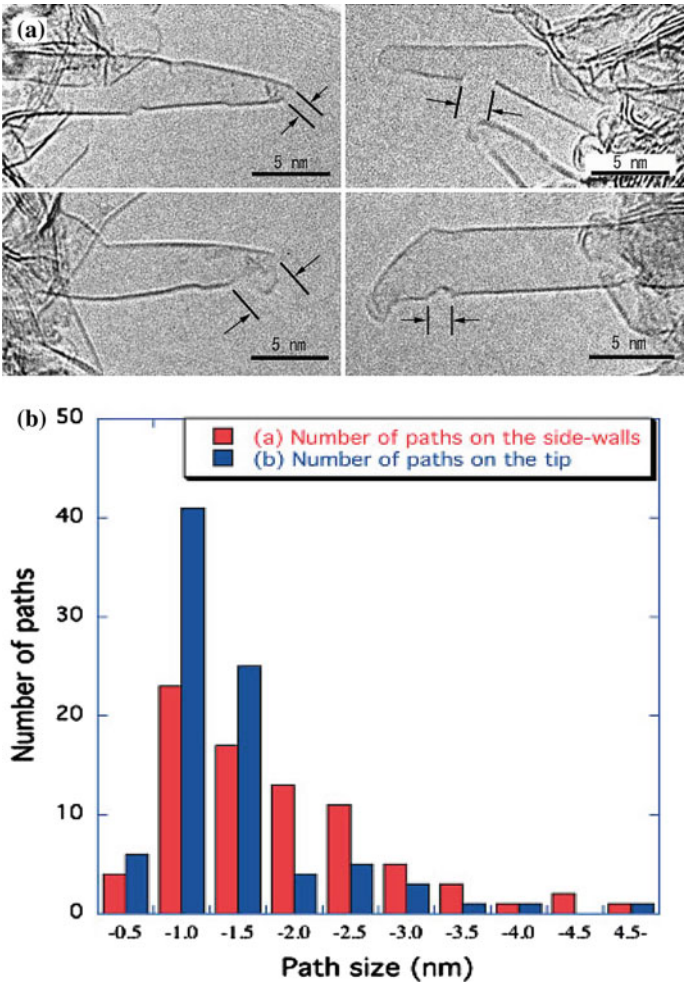

Fig. 4 **a** TEM images of SWNHs after heat treatment in O_2. The pathway holes are clearly visible at the nanohorn tips and sidewalls. **b** Size distributions of the holes in the SWNH sidewalls (*red*) and tips (*blue*) [19]

1.3 Isolation of SWNHs from Aggregates

As described above, as-grown SWNH aggregates are assembled from thousands of individual SWNHs. The individual nanoparticles in these aggregates are held together by strong forces, and cannot be separated without difficulty. However, the individual SWNHs or small-sized carbon nanohorns can be readily isolated by ultrasonication, followed by density gradient centrifugation [25, 26]. To separate individual SWNHs, oxidized SWNH aggregates are dispersed in a surfactant of

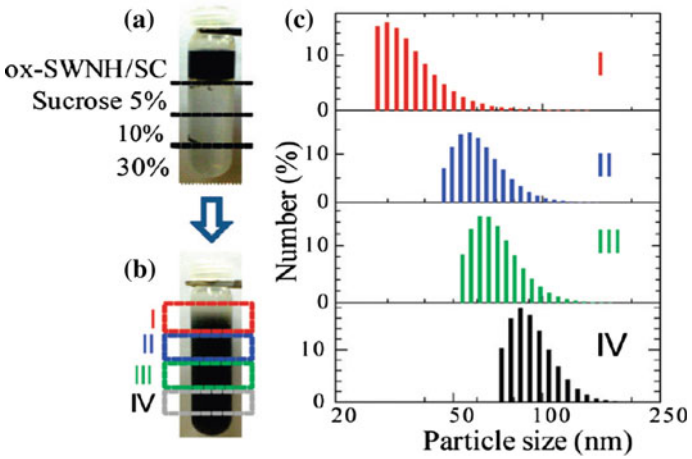

Fig. 5 **a** Centrifuge tube containing a sodium cholate dispersion of an oxidized SWNH aggregate (ox-SWNH) placed on top of a sucrose gradient made up of three layers with varying sucrose concentrations (5, 10, and 30 %). **b** The same tube after centrifugation for 4 h at 4600 × g. Four zones are illustrated (I–IV). **c** Size distributions of the particles in layers I–IV. Particle diameters were measured by dynamic light scattering [26]. Ox-SWNH/SC, oxidized SWNH aggregate/sucrose

sodium dodecylbenzenesulfonate by ultrasonication, and then subjected to sucrose density gradient centrifugation (Fig. 5a) [26]. This treatment yields three populations of SWNHs: individual SWNHs and SWNH aggregates with a diameter of ~30–40 nm at the top of the centrifuge tube (layers I Fig. 5b), SWNH aggregates with a diameter of ~70 nm in the middle of the centrifuge tube (layers II and III), and SWNH aggregates with a diameter of ~100 nm at the bottom of the centrifuge tube (layer IV). The shapes of the individual SWNHs correspond to straight and two- and three-way branched forms. The lengths of the straight SWNHs and each arm of the branched forms are about 10–70 nm, and their diameters are about 2–10 nm (Fig. 6).

Similar structures of small-sized SWNHs in larger quantities (yield >20 %) can be successfully separated by a surfactant-free oxidation protocol [27], which is similar to Hummer's oxidative exfoliation technique for graphene oxide separation from graphite [28]. The particle sizes of the obtained small-sized SWNH aggregates (S-SWNHs) are ~20–50 nm, as estimated by dynamic light scattering (Fig. 7a) [27]. The typical morphologies of the S-SWNHs and accompanying large-sized SWNH aggregates (L-SWNHs, ~80–120 nm) are shown in the TEM images in Fig. 7b. S-SWNHs obtained by this oxidation method are hydrophilic, and show stable dispersion in aqueous solutions (Fig. 7a, inset).

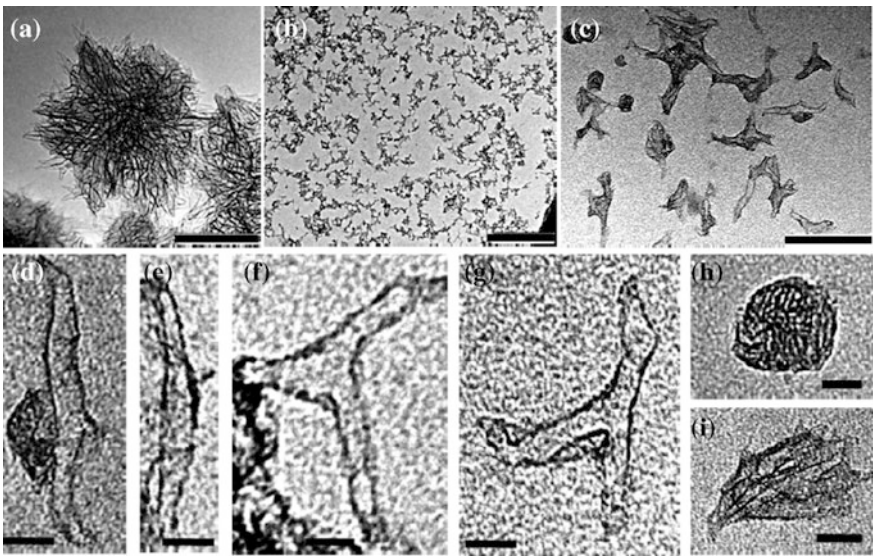

Fig. 6 **a** Typical TEM image of an oxidized SWNH aggregate. **b**, **c** TEM images of the particles in layer I (Fig. 5b). **d**, **e** TEM images of straight particles. **f**, **g** TEM images of branched forms. **h**, **i** TEM images of small aggregates. Scale bars, 50 nm (**a**, **b**), 100 nm (**c**), and 10 nm (**d**–**i**) [26]

1.4 Surface Functionalization

Covalent modification SWNHs have a hydrophobic graphite surface, which limits their applications in biological research fields. Many efforts have been made to change the nanohorn surface from hydrophobic to hydrophilic by functionalization with hydrophilic groups. The treatment of SWNHs with strong acids (e.g., HNO_3 or sulfuric acid (H_2SO_4), either singly or in combination) [15, 21, 22, 29] induces the formation of defects or holes, and also generates numerous carboxyl, carbonyl, and other oxygenated groups at the site of the defects and the edges of the holes. Hydrogen peroxide (H_2O_2)-mediated oxidation assisted by light irradiation also effectively generates carboxylic groups on the SWNH surface [21]. The carboxylic groups are then reacted via amidation with amino-containing compounds, including proteins (e.g., bovine serum albumin (BSA)), organic amines, alcohols, and thiols [22, 30, 31]. The obtained BSA-SWNHs exhibit high biocompatibility, stable dispersion in aqueous solutions, and good cell entry by endocytosis without cytotoxicity [22].

Another kind of chemical functionalization is initiated through the modification of as-grown SWNH sidewalls by direct attack of an amine (nucleophilic addition) [31, 32] or by 1,3-dipolar cycloaddition [33, 34]. The reacted SWNH derivatives show high solubility in common organic solvents, such as chloroform, dimethylformamide [33], and toluene [34].

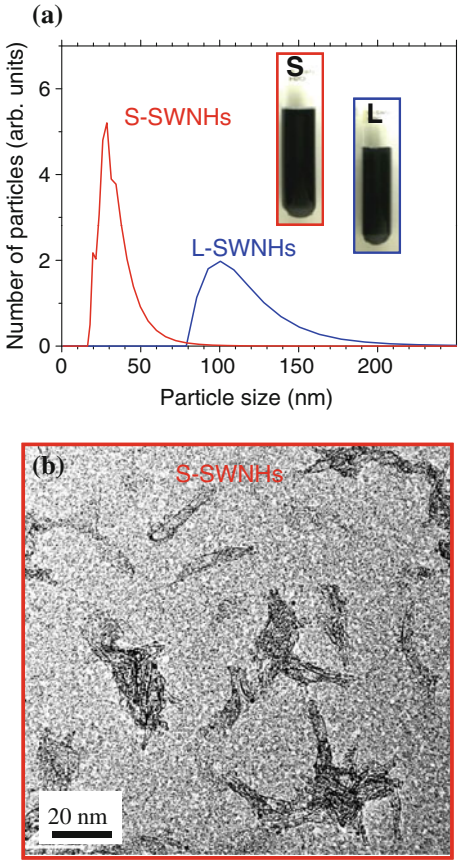

Fig. 7 **a** Dynamic light scattering measurements of aqueous dispersions of S-SWNHs and L-SWNHs. **b** TEM images of S-SWNHs [27]

Noncovalent coating. Noncovalent coating of SWNHs with polyethylene glycol (PEG)-based amphiphilic molecules can disperse nanohorn aggregates in aqueous solutions due to the hydrophilic properties of the PEG moieties. Physical modification of SWNHs with PEG successfully reduces non-specific adsorption of proteins onto SWNHs [35–38]. Different types of PEG-based macromolecules show different dispersion capabilities toward SWNH aggregates [37, 38].

1.5 Photo-Thermal Conversion Efficiency of SWNHs

SWNHs exhibit high photo-thermal energy conversion efficiency and high absorption cross-sections in a 650–1100-nm wavelength region of the so-called diagnostic window [39–46]. Oxidized SWNH particles complexed with BSA (SWNHox-BSA) and dispersed in aqueous solutions can effectively convert light energy into thermal energy [39, 40]. The temperature changes accompanying

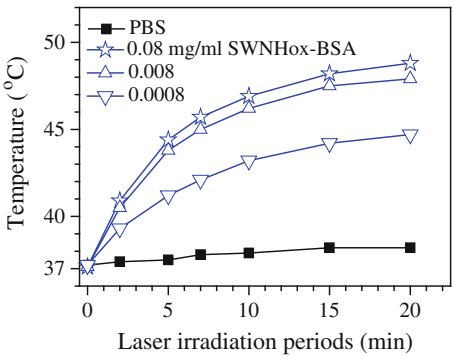

Fig. 8 Temperature increases of PBS alone and PBS dispersions of SWNHox-BSA particles upon irradiation with a 670-nm laser [39]

SWNHox-BSA dispersion (SWNH concentration = 8 μg/mL in phosphate buffered saline (PBS)) exhibit a temperature increase of ~10 °C upon irradiation with a 670-nm laser irradiation for ~10 min [39], whereas a control PBS solution without the SWNHox-BSA complex shows no such increase in temperature (Fig. 8).

2 Application of SWNHs in Biological Research Fields

2.1 Drug Delivery

SWNHs are regarded as promising carriers in drug delivery systems [47–54] due to the following characteristics. First, the nanohorns have large surface areas and total pore volumes, enabling abundant adsorption or storage of guest molecules. Second, SWNHs are spherical aggregates with diameters of ~100 nm, making them ideal for passive tumor-targeting conditions. Third, SWNHs can be produced in large quantities with high purity in the absence of metal catalysts, and in this way differ from carbon nanotubes. Drug incorporation inside an oxidized SWNHs (SWNHox) were initially demonstrated for dexamethasone (DEX) [47], an anti-inflammatory drug. Numerous DEX molecules were adsorbed onto the interior surface of the SWNHox, and the resultant DEX-SWNHox particle showed slow drug release kinetics, both in buffer solution and in cell culture medium.

The well-known anticancer agent, cisplatin (CDDP), can also be incorporated with up to 50 wt% of SWNHs efficiency inside the SWNHox particle to yield a CDDP@SWNHox delivery system (Fig. 9) [50]. The high anticancer efficacy of the derivatized particle has been tested in vitro and in vivo [49, 50], and stems from slow CDDP release from the SWNHox particle and a tendency of CDDP@SWNHox to attach to the cell surface. When CDDP@SWNH was locally injected into tumors, its anticancer actions were more pronounced than those of parental CDDP (Fig. 10), both due to slow drug release kinetics and the long particle retention time at the tumor site. These characteristics were attributed to the

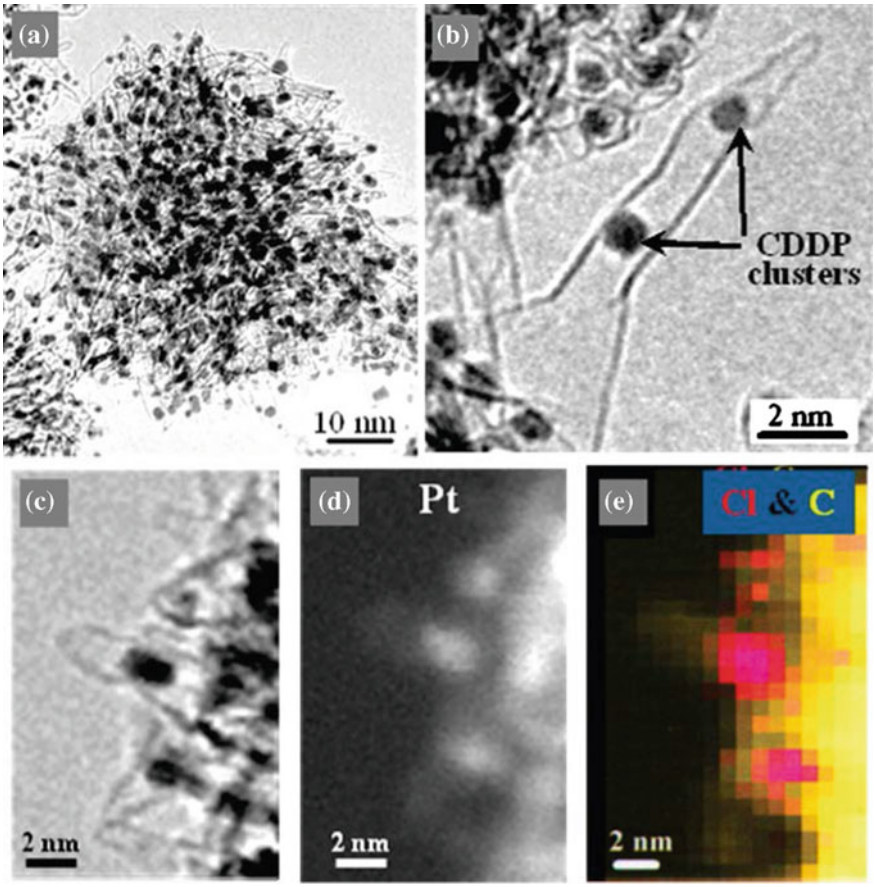

Fig. 9 TEM (**a**, **b**), scanning TEM (**c**), and Z-contrast (**d**) images of CDDP@SWNHox particles. C (carbon) and Cl (chloride) mapping was clarified by electron energy loss spectrum measurements (**e**). Observations or measurements of the images (**c**, **e**) were fixed at the same area. *Black* particles (**a**, **c**) indicate CDDP clusters. Two CDDP clusters within one CNHox sheath are indicated by *arrows* in (**b**). *Bright spots* in (**d**) correspond to platinum (Pt) atoms in the CDDP clusters. *Yellow* and *magenta* areas in (**e**) indicate the presence of C and Cl, respectively [50]

size of the CDDP@SWNHox particle, which precluded its ready drainage through the lymphatic system [50].

2.2 Use of SWNHs as Photo-Hyperthermia Agents

Besides their use as drug carriers, SWNHs are expected to be advantageous as photo-hyperthermia (PHT) agents for cancer therapy [39, 41, 46, and 55] and the

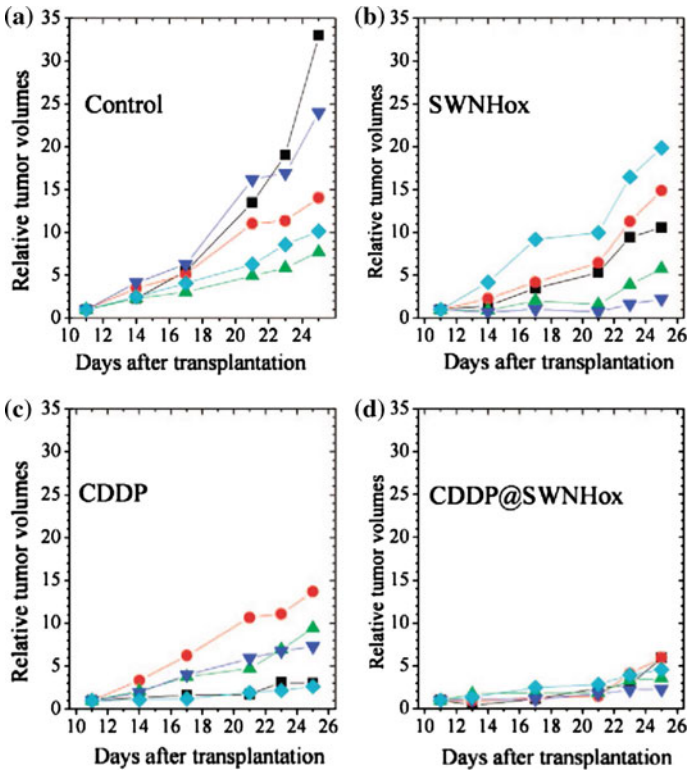

Fig. 10 Relative tumor volumes normalized at unity on day 11. Saline (**a**), SWNHox (**b**), CDDP (**c**), and CDDP@SWNHox (**d**) were intratumorally injected on day 11. The dosages of CDDP were 0.5 mg/kg. In each graph, the results of five mice are shown [50]

elimination of microbes [42] and viruses [43]. This is because the nanohorns absorb light in the phototherapy window (650–1100 nm), potentially transforming light energy into thermal energy and triggering cell death by a localized photo-thermal or PHT effect.

To evaluate the utility of SWNHs as PHT agents, a zinc phthalocyanine (ZnPc)-SWNHox-BSA conjugate was fabricated for the realization of such functions (Fig. 11). Here, ZnPc, a forthcoming agent for photodynamic therapy (PDT), was loaded inside and on the outer surface of a SWNHox with BSA attached to increase its biocompatibility [39]. Double PHT/PDT phototherapy with ZnPc-SWNHox-BSA particles and single-wavelength laser irradiation previously revealed the highly therapeutic impact of the derivatized biomaterial [39]. In in vivo tests, ZnPc-SWNHox-BSA was locally injected into tumors subcutaneously transplanted into mice. The nanohorn-loaded tumors were then subjected to laser irradiation (15 min/day for 10 days), prompting tumor disappearance (Fig. 12). These findings

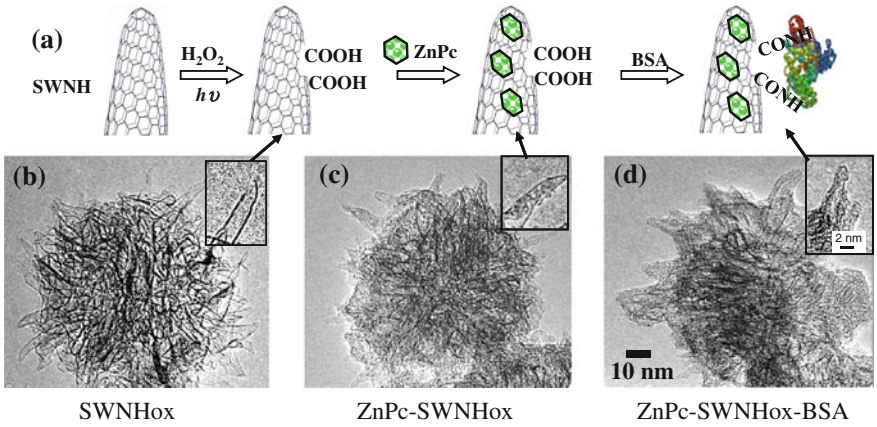

Fig. 11 Preparation of ZnPc-SWNHox-BSA particles. **a** Multistep production procedure. The nanohorns were visualized by TEM at each stage of production. **b** SWNHox, **c** ZnPc-SWNHox, and **d** ZnPc-SWNHox-BSA particles. *Insets* show magnified images [39]

were not replicated by ZnPc or SWNHox-BSA alone, suggesting that the enhanced antitumor efficiency was due to double phototherapy.

The photodynamic mechanism of ZnPc-SWNHox-BSA was investigated in detail via photophysical studies [39, 55]. Excitation of ZnPc by light-stimulated electron transfer to the SWNHox particle engenders a charge-separation state in the ZnPc-SWNHox-BSA system. In the presence of oxygen, electrons from the charge-separated ZnPc-SWNHox-BSA particle are transferred to O_2 to generate $O_2^{\bullet -}$ with the subsequent production of additional reactive species, such as hydroxyl radicals. The presence of these reactive species can then instigate the death of nearby cancer cells [39]. The photochemical processes involving ZnPc-SWNHox-BSA under aerobic conditions are illustrated in Fig. 13 [39, 55].

2.3 *Photo-Thermal Conversion Engineering*

The characteristics of photo-thermal energy conversion might also be useful in gene expression engineering [40], or the production of photoinduced nanomodulators for selective eradication of microbes [42]. In this regard, BSA-SWNHs can supply the thermal energy necessary for heat shock promoter-mediated gene expression when introduced into various cells and transgenic medaka (*Oryzias latipes*) [40].

Recently, functionalization of SWNHs with an infrared dye, IRDye800CW, permitted the fabrication of a light-driven nanomodulator for controlling calcium ion flux and membrane currents at the single-cell level [56]. IRDye800CW was chosen for labeling the nanohorns as it can generate reactivate oxygen species (ROS) through near infrared (NIR) light absorption, and promote successive

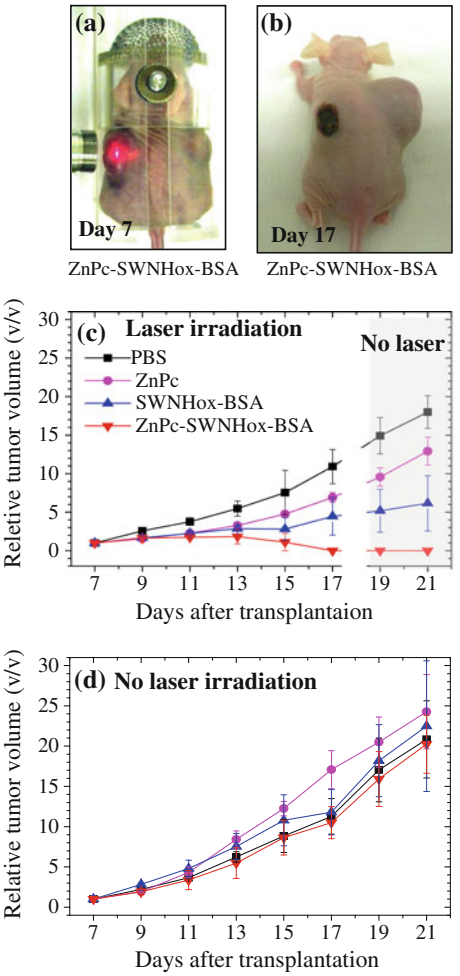

Fig. 12 Photodynamic and hyperthermic destruction of tumors in vivo. **a** A mouse with large tumors on the left and right flank is shown at 7 days after tumor cell transplantation (day 7). **b** A mouse after 10 days of treatment (day 17) with intratumorally-injected ZnPc-SWNHox-BSA particles and 670-nm laser irradiation of the tumor on the left flank. **c** Relative volume of the tumor on the left flank (volume after irradiation/volume before irradiation) following injection with PBS (*black line*) or PBS dispersions of ZnPc (*magenta line*), SWNHox-BSA particles (*blue line*), or ZnPc-SWNHox-BSA particles (*red line*) and irradiation with a 670-nm laser. **d** Relative volume of the tumor on the right flank following injection with PBS (*black line*) or PBS dispersions of ZnPc (*magenta line*), SWNHox-BSA particles (*blue line*), or ZnPc-SWNHox-BSA particles (*red line*), but not subjected to laser irradiation [39]

electron/energy transfer to the generated ROS [39, 55, 57, 58]. ROS-mediated regulation of calcium and other ion channel activities plays a central role in many free radical-driven processes, including stress, hormone signaling, and immunological responses.

After labeling with IRDye800CW, the obtained dye-labeled SWNHs (dye-SWNHs) generated both heat and ROS. Mouse neuroblastoma-derived ND7/23 hybrid cells were used to study the actions of dye-SWNH, because these cells express temperature-activated transient receptor potential ion channels (thermo-TRPs) and calcium ion channels (e.g., the inositol triphosphate (IP3) receptor). Incubation of ND7/23 cells with dye-SWNHs and irradiation with a NIR laser caused a local temperature increase, generation of high ROS levels, and the opening of thermo-TRPs and calcium ion channels. Channel opening then caused an influx and/or release of Ca^{2+} from intracellular compartments (Fig. 14a) [56].

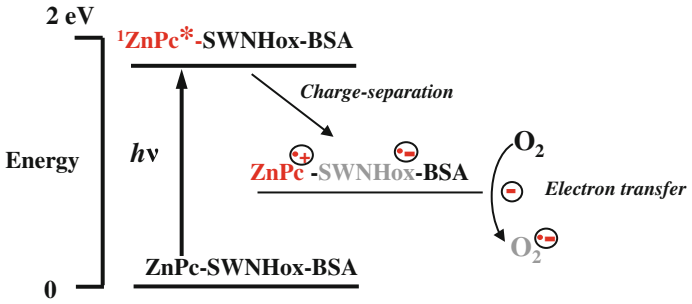

Fig. 13 Photochemical processes involving ZnPc-SWNHox-BSA in the presence of O_2. Under aerobic conditions both in vivo and in vitro, O_2 accepts an electron from the charge-separated ZnPc-SWNHox-BSA particle, generating $O_2^{\bullet-}$ [39, 55]

Next, the authors confirmed whether the nanomodulator-generated local temperature and ROS content were sufficiently increased to regulate channel activity. This was done by observing intracellular calcium flux through the use of a fluorescent calcium probe, Fluo-8. Following internalization of dye-SWNH nanomodulators into ND7/23 cells and cellular irradiation at 808 nm (laser power = 204 μW, or ~104 μW/μm^2), a bright green fluorescence due to calcium influx was observed. Fluo-8 fluorescence intensity was diminished in low TRP-expressing RAW264.7 and HeLa cells relative to ND7/23 cells, and fluorescence intensity was also reduced for dye-only and SWNH-only controls (Fig. 14b) [56].

Laser-triggered remote bioexcitation was further investigated in a model of a *Xenopus laevis* paw (Fig. 15) [56]. *X. laevis* have nerves that express thermo-TRPs and a variety of other channel proteins [59]. NIR light can penetrate into the tissue for a distance of ≤10 cm [60], allowing noninvasive excitation of dye-SWNH nanomodulators within a significant area of the thigh. Dye-SWNHs were injected under the thigh of a euthanized frog. Immediately after the initiation of irradiation (wavelength = 800 nm; laser power = 2.1 W, or ~292 mW/mm^2), paw twitching was observed. The same movement was absent when underivatized NH2-SWNHs, IRDyeCW800 alone, or Ringer solution alone without SWNHs was injected. These results indicate that dye-SWNHs can mediate cell stimulation in *X. laevis* tissues, facilitating significant bioexcitation [56].

2.4 Biosensor Applications

SWNHs are useful in electrochemical and biosensor applications [61–66], because they are metal-free, biocompatible, easily functionalized, and possess very large surface areas. Xu and colleagues first reported the use of SWNHs for construction of a glucose biosensor in 2008 [61]. The authors fashioned a biosensor by encapsulating glucose oxidase in a Nafion-SWNHs composite film. Ferrocene monocarboxylic acid was used as a redox mediator to decrease detection potential.

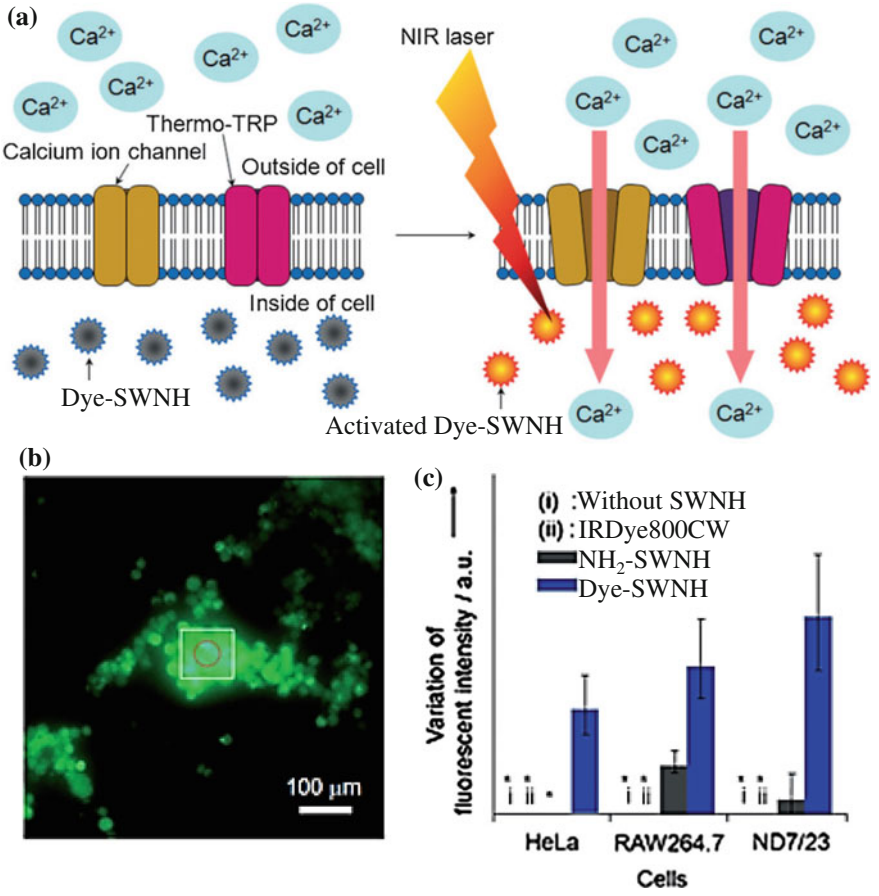

Fig. 14 Cellular stimulation by nanomodulators. **a** Illustration of the control of cellular activity by photoinduced nanomodulators. **b** Calcium imaging in ND7/23 cells incubated with dye-SWNHs, as assessed by fluorescence emission of the calcium probe, Fluo-8, after laser irradiation. The *white square* shows the site of fluorescence analysis, and the *red circle* indicates the irradiated site. **c** Analysis of fluorescence emission by irradiated cells with internalized dye-SWNHs. *No significant difference in fluorescence intensity [56]

The mediated biosensor demonstrated good electro-catalytic activity toward oxidation of glucose, and showed a linear range from 0 to 6.0 mM. The biosensor also showed high sensitivity (1.06 μA/mM) and stability, and avoided the commonly coexisting interference. Later, the same group reported development of a H_2O_2 biosensor based on the direct electrochemistry of SWNHs noncovalently modified with soybean peroxidase and deposited on a modified electrode surface [62]. This biosensor exhibited high sensitivity (16.625 μAL/mmol) with a detection limit of 5.0×10^{-7} mmol/L and excellent stability, indicating that noncovalent

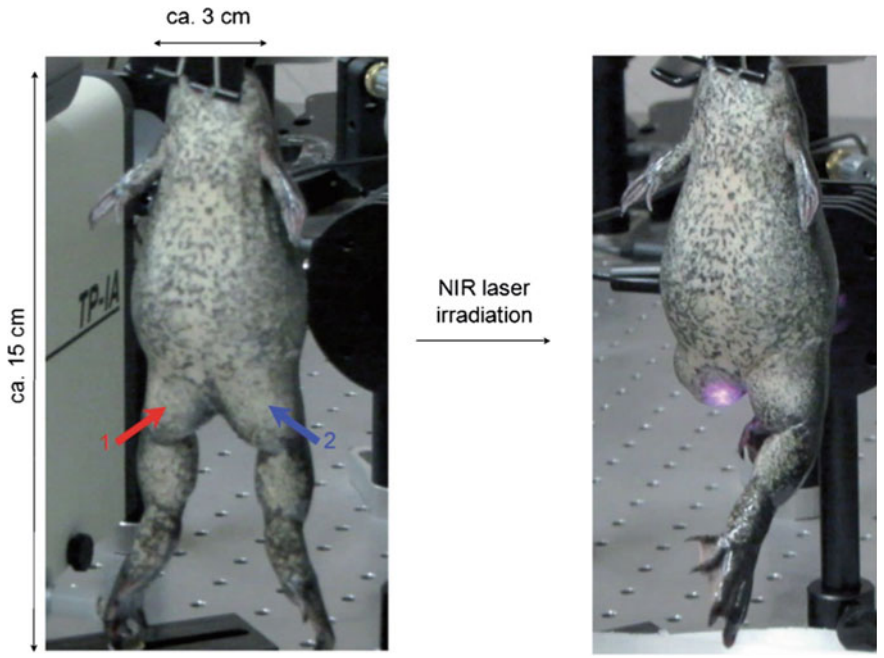

Fig. 15 Laser-driven remote stimulation of a frog (*X. laevis*) before (*left*) and after (*right*) laser irradiation. *Red* and *blue arrows* show the location of dye-SWNH (1) and Ringer solution (2) injection. Sample concentrations of dye-SWNH, NH_2CNH, and IRDye800CW were 300, 225, and 75 mg/mL, respectively [56]

functionalization of SWNHs can facilitate their applications in biosensor and electrochemistry research fields.

Recently, sensitive electrochemical immunosensors incorporating SWNHs were developed for detection of toxins, glycoproteins, and cancer biomarkers [64–66]. For example, SWNHs were functionalized by covalently binding microcystin-LR (MC-LR) to the carboxylic groups on the nanohorn tips for MC-LR toxin-detection (Fig. 16) [64]. An antibody against horseradish peroxidase (HRP)-labeled MC-LR was then prepared and utilized in a competitive immunoassay. Subsequently, the immunosensor exhibited a wide linear response to MC-LR under optimal conditions, ranging from 0.05 to 20 μg/L with a detection limit of 0.03 μg/L at a signal-to-noise ratio of 3, which was much lower than the World Health Organization/WHO provisional guideline limit of 1 μg/L for MC-LR in drinking water [67]. These results suggest that SWNHs can provide a useful platform for preparation of immunosensors for small-toxin molecules, which could readily be extended toward the on-site monitoring of hazardous components in food and environmental matrices.

Toward the detection of cancer biomarkers, a novel sandwich-type electrochemical immunosensor based on functionalized nanomaterial labels and bi-enzyme

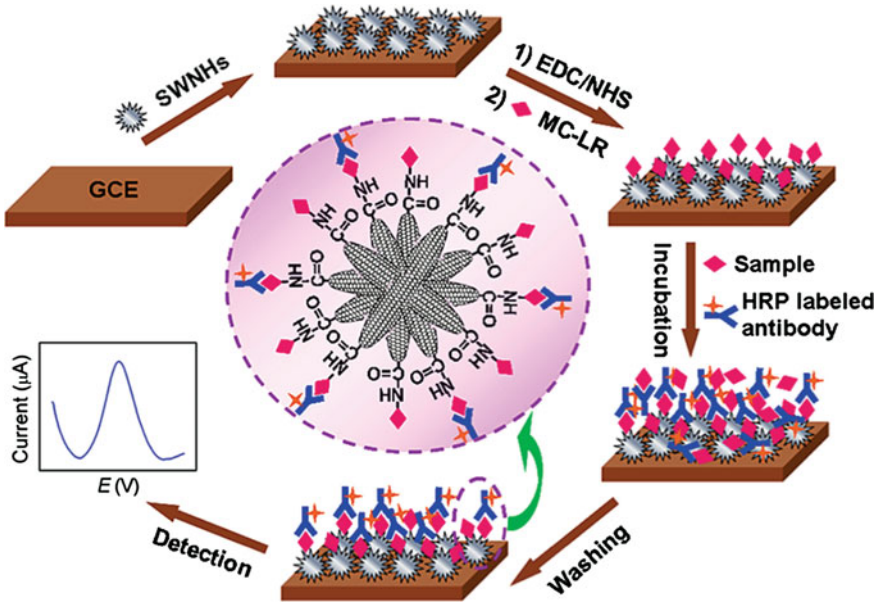

Fig. 16 Preparation and detection procedures for the MC-LR immunosensor by using functionalized SWNHs. EDC, 1-ethyl-3-(3-dimethylaminopropyl)carbodiimide; NHS, N-hydroxysuccimide [64]

(horseradish peroxidase and glucose oxidase)-catalyzed precipitation was developed for the detection of α-fetoprotein (AFP) [66]. The enzymes were linked to functionalized SWNHs and used as biocatalysts to accelerate 4-chloro-1-naphthol oxidation by H_2O_2 to yield a insoluble precipitate on the electrode surface. Mass loading of the precipitate led to a significantly enhanced signal relative to conventional loading techniques. Under optimal conditions, the immunosensor showed high sensitivity with a low detection limit of 0.33 pg/mL, and a wide linear range from 0.001 to 60 ng m/L. The immunosensor also exhibited good selectivity, acceptable stability, and good reproducibility. Therefore, the proposed amplification strategy described in Ref. [66] is promising for SWNH-based clinical screening of tumor biomarkers.

3 SWNH Toxicity and Biodegradation

3.1 Toxicity

The toxicity of SWNHs, SWNHoxs, and their functionalized forms has been investigated in vitro and in vivo [22, 32, 46–54]. Importantly, no serious cell death was found in in vitro cellular viability assessments. Tailored toxicity tests [58]

Table 1 SWNH toxicological tests [68]

Test	Test organism/animal	Dosage	Findings
Reverse mutation (Ames) test	S. typhimurium and *E. coli* strains	78–1250 g/plate	No positive increase in revertants; no growth inhibitory effect
Chromosomal aberration test	Chinese-hamster lung fibroblast cell line	0.010–0.078 or 0.313–2.5 mg/mL	Negligible positive incidences of structural chromosomal aberrations or polyploidy
Skin primary irritation test	Rabbits	0.015 g/site	Primary irritation index (P.I.I.) = 0; no clinical signs of abnormalities; normal body weight gain
Eye irritation test	Rabbits	0.02 g/eye	Draize irritation score = 0; no clinical signs of abnormalities; normal body weight gain
Skin sensitization (adjuvant and patch) test	Guinea pigs	0.02 g/site (induction); 0.01 g/site (challenge)	Mean response score 0; no clinical signs of abnormalities; normal body weight gain
Peroral administration test	Rats	2000 mg/kg	No mortality; no clinical signs of abnormalities; normal body weight gain
Intratracheal instillation test	Rats	2.25 mg/animal (17.3 mg/kg)	No mortality; rale for all animals including control group; normal body weight gain; black lung spots and anthracosis; foamy macrophage in intra-alveolar spaces

likewise showed no abnormal signs in animals (Table 1); and histological studies, blood tests, and cytokine measurements showed no appreciable abnormalities in most organs [69, 70], hematological outcomes, or immune responses [70] after intravenous injection of functionalized SWNHs and SWNHoxs.

The availability of large quantities of SWNHs was exploited by assessing cytotoxicity and immune responses following the abundant uptake of these structures by RAW264.7 murine macrophages [71]. High cellular uptake of the nanohorns was accompanied by localization of SWNHs at lysosomes, destabilization pf lysosomal membranes, and ROS generation with ensuing apoptotic and necrotic cell death. Despite these findings, only low levels of cytokines were released by the SWNH-loaded macrophages [71]. Next, the nanohorn-triggered cell death process was investigated in more detail to identify an underlying mechanism of ROS-provoked apoptosis [72]. The results showed that SWNHs accumulated in the lysosomes of RAW264.7 macrophages, where they induced lysosomal membrane permeabilization and the subsequent release of cathepsins and other lysosomal proteases, in turn triggering mitochondrial dysfunction and production of ROS in the mitochondria. Nicotinamide adenine dinucleotide phosphate oxidase was not directly involved in SWNH-directed ROS production, and ROS generation was not

regulated by the mitochondrial electron transport chain. An ROS feed-back loop further amplified the mitochondrial dysfunction, leading to the activation of caspases and cell apoptosis [72].

3.2 Biodistribution

Labeling of SWNHs with gadolinium(III) oxide (Gd_2O_3) Although SWNHs show high potential for use in drug delivery systems and other biomedical applications [46–54], several issues must be addressed prior to their practical employment. These issues include SWNH biodistribution, excretion, and degradation, and bring into question not only the safety of SWNHs, but also the efficiency of in vivo nanohorn delivery. SWNHs have no unique characteristics that are useful for detection, and thus, they cannot be easily quantified in cells or whole-body systems based on intrinsic properties. To overcome this problem, a Gd_2O_3 label was incorporated into SWNHs to yield Gd_2O_3@SWNHs through holes opened by oxidation [73–77]. The holes were closed by heat treatment after Gd_2O_3 incorporation, permitting stable labeling of the biomaterial without leaching of Gd_2O_3 into the surrounding biological environment.

Measurement of Gd content in Gd_2O_3@SWNHs by inductively coupled plasma atomic emission spectroscopy (ICP-AES) permitted an estimation of nanohorn accumulation in every mouse organ and tissue [76]. In addition, the embedded Gd_2O_3 in the SWNH aggregates also facilitated ultrastructural localization of SWNHs by TEM, because Gd is not found naturally within the body. The high electron-scattering ability of Gd provided high contrast for clear detection by TEM (Fig. 17), and energy dispersive X-ray spectroscopy (EDX) or electron energy loss spectroscopy (EELS) further assisted in the identification of the SWNH aggregates. TEM coupled with elemental analysis by EDX and EELS is a conventional technique for localizing fine particles derived from various materials in living tissues [78–81].

Biodistribution of SWNHs with glucose-coating Gd_2O_3@SWNHs were dispersed in glucose and intravenously injected into mice. The Gd_2O_3@SWNHs were rapidly entrapped by the liver and the spleen, and these organs retained 70–80 and 10 % of the initially injected dose, respectively, in <30 min. Ultrastructural localization of Gd_2O_3@SWNHs in the murine liver revealed their presence in cellular phagosomes and phagolysosomes [76].

Biodistribution of SWNHs with PEG coating In another experiment, our research group dispersed Gd_2O_3@SWNHs into a solution of DSPE-PEG to enhance the stealth properties of SWNHs. As expected, the PEG-coated Gd_2O_3@SWNHs had a relatively long circulatory half-life (5–6 h) (Fig. 18a) after intravenous injection into mice [77] compared with SWNHs dispersed in glucose [76].

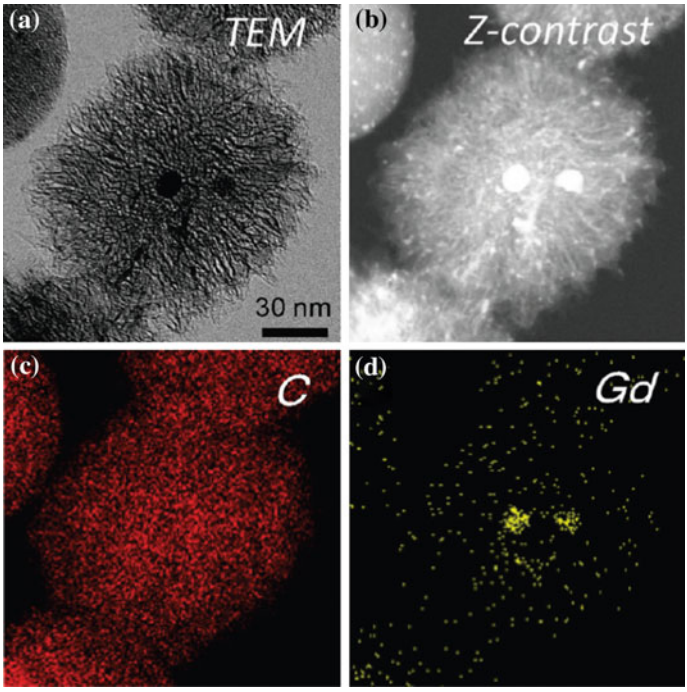

Fig. 17 Microscopic structure of the Gd_2O_3@SWNH powder. **a** TEM images and **b** Z-contrast images. **c** Carbon (C) and **d** Gd maps measured in the same area shown in (**a**) and (**b**) [76]

To understand the fate of SWNHs within the body, we analyzed SWNH content in the whole body and every organ of the mouse at seven time points over a period of 4 months. SWNH contents in various organs as a percentage of the initial dose are shown in Fig. 18b. SWNH content in the liver increased and reached a maximum of ~70 % at a post-injection time (PIT) of 24 h, before decreasing to ~30 % at a PIT of 30 days. Thereafter, no further appreciable changes in SWNH content were observed up until the end of the study period (120 days) (Fig. 18b). The changes in nanohorn content were paralleled by color changes in the liver; namely, the liver became gradually darker in color from PIT 1–24 h due to the presence of labeled SWNHs, but gradually returned to baseline color at PIT 30 d, with little change occurring thereafter. SWNH content in the spleen increased from 6 % at 1 h to 10 % at 7 days, with little change discerned after the first week of the experiment. SWNH content in the kidney was ~3–5 % throughout the study period. No darkening of the kidney tissue was observed, but histological observations revealed black particles in the renal corpuscles [77].

SWNH content and associated color deposition showed no significant changes in other parts of the body during the observation period, including the heart, lung, and stomach (Fig. 18b). Interestingly, SWNH content in the whole body of the mouse decreased to 60 % at a PIT of 30 days, with no further changes at later times. These

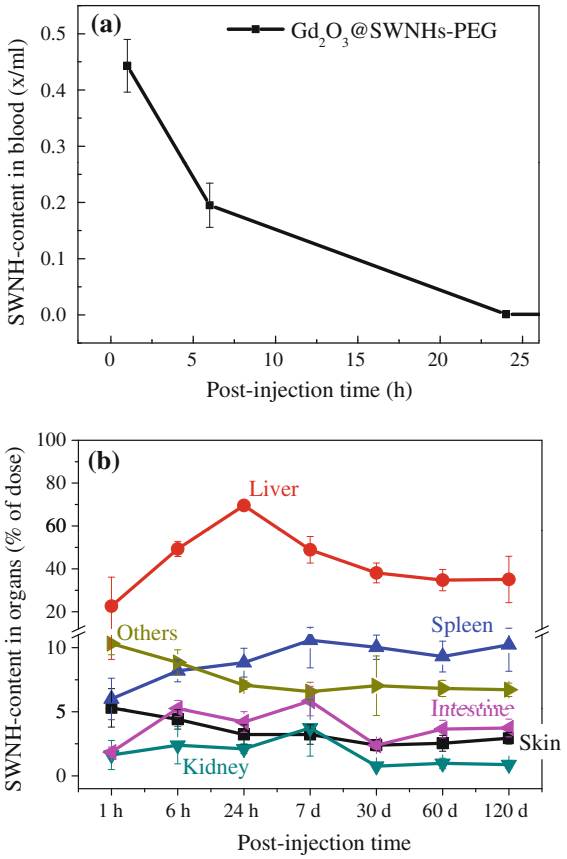

Fig. 18 **a** Blood-circulation behavior and **(b)** biodistribution of Gd_2O_3@SWNHs-PEG in the whole body of the mouse from 1 h to 4 months after a single intravenous injection of the biomaterial (dose = 5 mg/kg). **b** SWNH content in tissues and organs was determined by measuring the Gd content via ICP-AES. All data are given as a percentage of the original total injected dose (means ± the SD, n = 5) [77]

results signify that ~40 % of the injected SWNH dose was lost from the mouse body within 30 days (Fig. 19a). SWNH content in the feces was also measured, and was found to be ~15 % of the original dose at 60 days post-injection (Fig. 19b). We presumed that the other 25 % of the original dose lost from the body was degraded.

Size-dependent biodistribution The biodistribution of SWNHs administered to mice seems to depend on particle or aggregate size [70]. Two different sizes of SWNH aggregates (30–50-nm aggregates (S-SWNHs) and 80–120-nm aggregates (large-sized SWNH aggregates, or L-SWNHs)) were used to investigate nanohorn biodistribution and toxicity by histological analysis and blood testing for 7 days after intravenous injection into mice. Consequently, S-SWNHs accumulated more slowly in the liver and the spleen than L-SWNHs (Fig. 20), suggesting a longer time spent circulating in the blood.

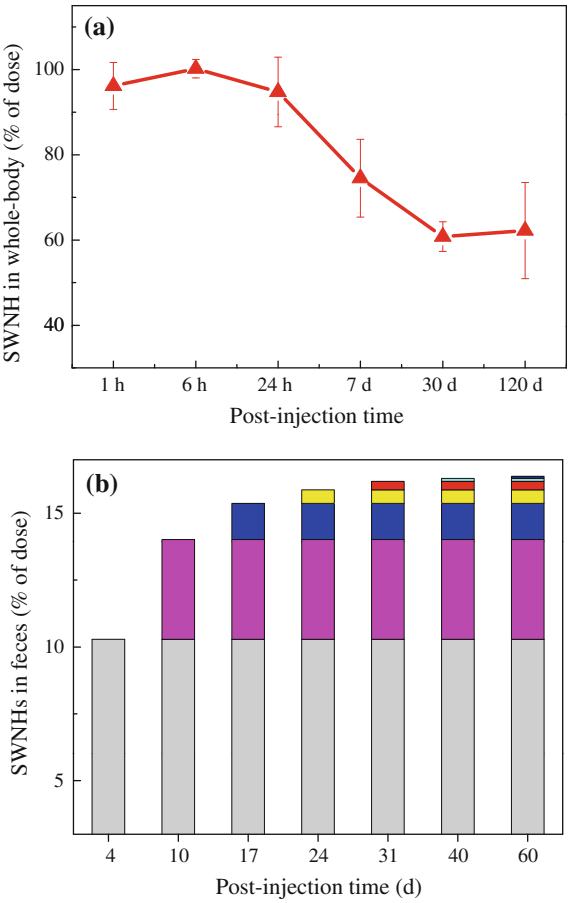

Fig. 19 **a** SWNH content in the whole body of the mouse after a single intravenous injection of Gd2O3@SWNHs-PEG from PIT 1 h to 4 months. Data are given as the means ± the SD (n = 5). **b** Average SWNH content in the feces collected from PIT 4 days to 2 months after a single intravenous injection of Gd2O3@SWNHs-PEG (n = 5) [77]

3.3 Biodegradation

Historically, carbon nanomaterials have been generally regarded as non-biodegradable in tissues due to their stable and inert graphitic structures; however, recent studies indicate that peroxidase-based enzymatic processes facilitate the oxidation and biodegradation of carbon nanotubes (CNTs) and graphene by cells and cell-derived catalysts [82–91]. For instance, oxidized SWNTs were enzymatically degraded by stimulated neutrophils without causing obvious pulmonary inflammation when the products of degradation were instilled in the lungs [84, 91].

Another study investigated SWNH degradation via enzymatic oxidation by isolated macrophage-derived myeloperoxidase (MPO) [92]. Here, SWNH dispersions were treated with a solution of human MPO supplemented with a low concentration of H_2O_2 (800 μM). The dark dispersion of MPO-/H_2O_2-treated SWNHs gradually lightened over 24 h, while the dark color of a control H_2O_2-treated

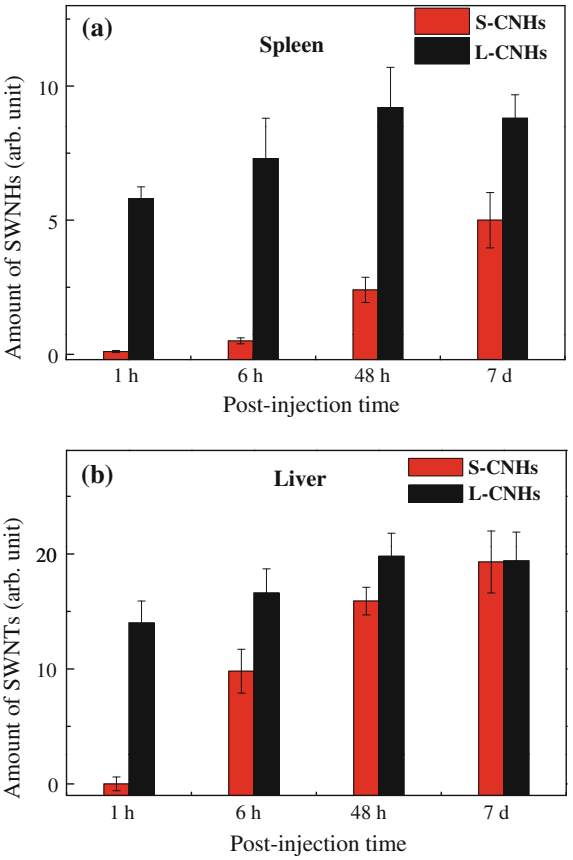

Fig. 20 Amount of S- (30–50 nm) and L-SWNH (80–120 nm) accumulation in the spleen (**a**) and liver (**b**) obtained by measurement of pigmented areas in images of tissue sections. All data are given as the means ± the SD (n = 5) [70]

SWNH dispersion showed no such change during the same time period (Fig. 21a). Optical absorption measurements [92] revealed that SWNH content decreased by approximately 40 wt% and 60 wt% after treatment with a combination of MPO and H_2O_2 for 5 h and 24 h, respectively (Fig. 21b). Additionally, TEM images showed that any SWNHs remaining after enzymatic oxidation for ~24 h were severely damaged, with collapse of the horn-shaped tips and spherical forms. The structures of the incompletely degraded SWNHs resembled amorphous carbon or graphite-like carbon nanoparticles [90], implying that MPO-mediated biodegradation occurs from the aggregate periphery to the center.

The cellular degradation of SWNHs by RAW 264.7 macrophages and THP-1 monocyte-derived macrophages was also investigated in vitro. The cells were incubated for 24 h with SWNHox (10 μg/mL), washed with PBS, and then re-seeded with SWNH-free fresh culture medium for an additional 1–9 days (recovery period). Images of the THP-1 cells after the recovery period showed a reduction in intracellular accumulation of SWNHs (Fig. 22a). Optical absorption

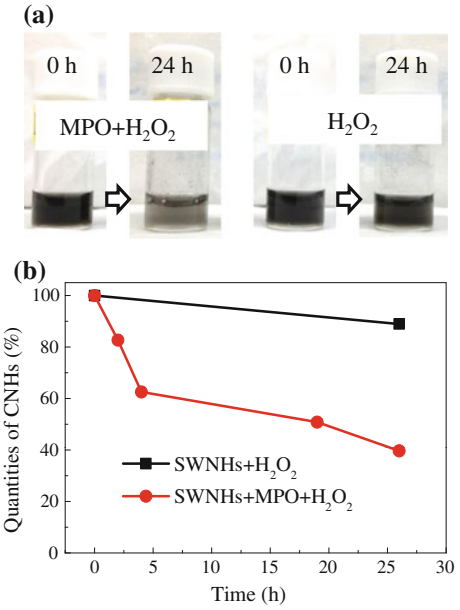

Fig. 21 Human MPO-mediated degradation of SWNHs. **a** Photographs of SWNH dispersions before and after treatment with 800 μM H_2O_2 in the presence or absence of MPO. **b** SWNH content as a percentage of the original dose after treatment with H_2O_2 in the presence or absence of MPO for the indicated time. SWNH content was determined based on optical absorbance at 700 nm [92]

measurements (shown for THP-1 cells in Fig. 22b) revealed that ~30 % of the internalized SWNHs disappeared within the 1–9-day time period for both macrophage cell lines [92].

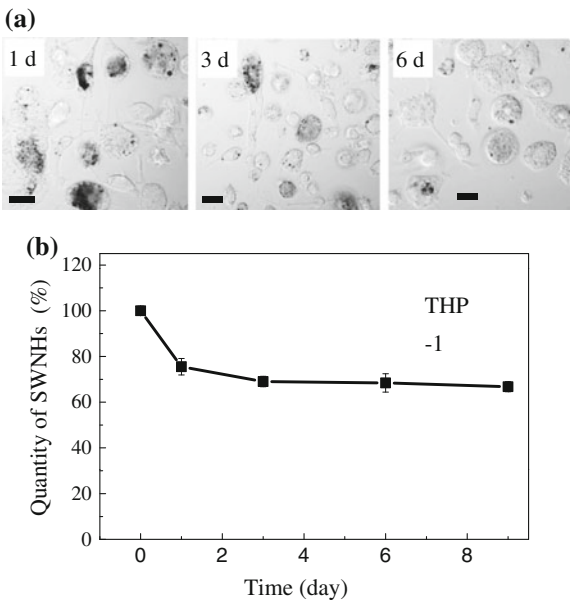

Fig. 22 Degradation of SWNHs in THP-1 monocyte-derived macrophages. Cells were differentiated by adding phorbol myristate acetate, incubated with SWNHs for 24 h, and then re-seeded in fresh medium without SWNHs and incubated for a further 1–9 days. **a** Confocal microscopy differential contrast images of THP-1 cells at days 1, 3, and 6. The black spots represent SWNHs. **b** SWNH accumulatation within the cells on days 1–9. Data represent SWNH content as a percentage of the original dose, and are given as the means ± the SD (n = 3 independent replicates) [92]

4 Perspectives and Challenges

In conclusion, SWNHs show great promise for use in biological research fields and diagnostic and therapeutic applications owing to their unique structure and associated physical properties. The pore geometry, photo-thermal transfer characteristics, and low toxicity of SWNHs offer potential solutions for many of the current challenges in the treatment of cancer, cardiovascular diseases, and other illnesses. However, numerous barriers still impede the practical employment of SWNHs. Although SWNHs show excellent drug-loading capabilities, the disease-targeting efficiency of the nanohorns is inferior relative to that of SWNTs. Additional efforts directed toward size control and the construction of multi-functional, SWNH-based drug delivery systems are required to increase the blood circulation time, accumulation ratio in tumor tissues, and biocompatibility of SWNHs. Furthermore, the prospective toxicity of SWNHs is not yet clear, especially in the long term, and SWNH excretion and degradation are difficult to study. Smaller-sized SWNH aggregates, as distinct from as-grown SWNHs, could possibly be used to circumvent at least some of these problems.

References

1. S. Iijima, M. Yudasaka, R. Yamada, S. Bandow, K. Suenaga, F. Kokai, K. Takahashi, Nano-aggregates of single-walled graphitic carbon nano-horns. Chem. Phys. Lett. **309**, 165–170 (1999). doi:10.1016/S0009-2614(99)00642-9
2. S. Iijima, T. Ichihashi, Single-shell carbon nanotubes of 1-nm diameter. Nature **363**, 603–605 (1993). doi:10.1038/363603a0
3. S. Iijima, Helical microtubules of graphitic carbon. Nature **354**, 56–58 (1991). doi:10.1038/354056a0
4. F. Kokai, K. Takahashi, D. Kasuya, M. Yudasaka, S. Iijima, Growth dynamics of single-wall carbon nanotubes and nanohorn aggregates by CO_2 laser vaporization at room temperature. Appl. Surf. Sci. **197–198**, 650–655 (2002). doi:10.1016/S0169-4332(02)00434-8
5. T. Azami, D. Kasuya, R. Yuge, M. Yudasaka, S. Iijima, T. Yoshitake, Y. Kubo, Large-scale production of single-wall carbon nanohorns with high purity. J. Phys. Chem. C **112**, 1330–1334 (2008). doi:10.1021/jp076365o
6. T. Yamaguchi, S. Bandow, S. Iijima, Synthesis of carbon nanohorn particles by simple pulsed arc discharge ignited between pre-heated carbon rods. Chem. Phys. Lett. **389**, 181–185 (2004). doi:10.1016/j.cplett.2004.03.068
7. N. Li, Z. Wang, K. Zhao, Z. Shi, Z. Gu, S. Xu, Synthesis of single-wall carbon nanohorns by arc-discharge in air and their formation mechanism. **48**, 1580–1585 (2010). doi:10.1016/j.carbon.2009.12.055
8. N. Sano, J. Nakano, T. Kanki, Synthesis of single-walled carbon nanotubes with nanohorns by arc in liquid nitrogen. Carbon **42**, 688–696 (2003). doi:10.1016/j.carbon.2003.12.078
9. H. Wang, M. Chhowalla, N. Sano, S. Jia, G.A.J. Amaratunga, Large-scale synthesis of single-walled carbon nanohorns by submerged arc. Nanotechnology **15**, 546 (2004). doi:10.1088/0957-4484/15/5/024
10. N. Sano, Low-cost synthesis of single-walled carbon nanohorns using the arc in water method with gas injection. J. Phys. D Appl. Phys. **37**, L17 (2004). doi:10.1088/0022-3727/37/8/L01

11. S. Bandow, F. Kokai, K. Takahashi, M. Yudasaka, L. Qin, S. Iijima, Interlayer spacing anomaly of single-wall carbon nanohorn aggregate. **321**, 514–519 (2000). doi:10.1016/S0009-2614(00)00353-5
12. D. Kasuya, M. Yudasaka, K. Takahashi, F. Kokai, S. Iijima, Selective production of single-wall carbon nanohorn aggregates and their formation mechanism. J. Phy. Chem. B **106**, 4947–4951 (2002). doi:10.1021/jp020387n
13. M. Inagaki, K. Kaneko, T. Nishizawa, Nanocarbons-recent research in Japan. Carbon **42**, 8–9 (2004). doi:10.1016/j.carbon.2004.02.032
14. K. Murata, K. Kaneko, F. Kokai, K. Takahashi, M. Yudasaka, S. Iijima, Pore structure of single-wall carbon nanohorn aggregates. Chem. Phys. Lett. **331**, 14–20 (2000). doi:10.1016/S0009-2614(00)01152-0
15. C. Yang, H. Noguchi, K. Murata, M. Yudasaka, A. Hashimoto, S. Iijima, K. Kaneko, Highly ultramicroporous single-walled carbon nanohorn assemblies. Adv. Mater. **17**, 866–870 (2005). doi:10.1002/adma.200400712
16. S. Utsumi, J. Miyawaki, H. Tanaka, Y. Hattori, T. Ito, N. Ichikuni, H. Kanoh, M. Yudasaka, S. Iijima, K. Kaneko, Opening mechanism of internal nanoporosity of single-wall carbon nanohorn. J. Phys. Chem. B **109**, 14319–14324 (2005). doi:10.1021/jp0512661
17. K. Murata, K. Kaneko, W. Steele, F. Kokai, K. Takahashi, D. Kasuya, K. Hirahara, M. Yudasaka, S. Iijima, Molecular potential structures of heat-treated Single-Wall Carbon Nanohorn Assemblies. J. Phys. Chem. B **105**, 10210–10216 (2001). doi:10.1021/jp010754f
18. J. Fan, M. Yudasaka, J. Miyawaki, K. Ajima, K. Murata, S. Iijima, Control of hole opening in single-wall carbon nanotubes and single-wall carbon nanohorns using oxygen. J. Phys. Chem. B **110**, 1587–1591 (2006). doi:10.1021/jp0538870
19. K. Ajima, M. Yudasaka, K. Suenaga, D. Kasuya, T. Azami, S. Iijima, Material storage mechanism in porous nanocarbon. Adv. Mater. **16**, 397–401 (2004). doi:10.1002/adma.200306142
20. E. Bekyarova, K. Kaneko, M. Yudasaka, D. Kasuya, S. Iijima, A. Huidobro, F. Rodriguez-Reinoso, Controlled opening of single-wall carbon nanohorns by heat treatment in carbon dioxide. J. Phys. Chem. B **107**, 4479–4484 (2003). doi:10.1021/jp026737n
21. C. Yang, D. Kasuya, M. Yudasaka, S. Iijima, K. Kaneko, Microporosity development of single-wall carbon nanohorn with chemically induced coalescence of the assembly structure. J. Phys. Chem. B **106**, 17775–17782 (2004). doi:10.1021/jp048391h
22. M. Zhang, M. Yudasaka, K. Ajima, J. Miyawaki, Sumio Iijima, Light-assisted oxidation of single-wall carbon nanohorns for abundant creation of oxygenated groups that enable chemical modifications with proteins to enhance biocompatibility. ACS Nano **1**, 265–272 (2007). doi:10.1021/nn700130f
23. T. Kawai, Y. Miyamoto, O. Sugino, Y. Koga, Nanotube and nanohorn nucleation from graphitic patches: Tight-binding molecular-dynamics simulations. Phys. Rev. B **66**, 033404 (2002). doi:10.1103/PhysRevB.66.033404
24. J. Miyawaki, R. Yuge, T. Kawai, M. Yudasaka, S. Iijima, Evidence of thermal closing of atomic-vacancy holes in single-wall carbon nanohorns. J. Phys. Chem. C **111**, 1553–1555 (2007). doi:10.1021/jp067283n
25. M. Zhang, M. Yudasaka, J. Miyawaki, J. Fan, S. Iijima, Isolating single-wall carbon nanohorns as small aggregates through a dispersion method. J. Phys. Chem. B **109**, 22201–22204 (2005). doi:10.1021/jp054793t
26. M. Zhang, T. Yamaguchi, S. Iijima, M. Yudasaka, Individual single-wall carbon nanohorns separated from aggregates. J. Phys. Chem. C **113**, 11184–11186 (2009). doi:10.1021/jp9037705
27. M. Zhang, X. Zhou, S. Iijima, M. Yudasaka, Small-sized carbon nanohorns enabling cellular uptake control. Sm Iijima all **8**, 2524–2531 (2012). doi:10.1002/smll.201102595
28. W. Hummer, R. Offeman, Preparation of graphitic oxide. J. Am. Chem. Soc. **80**, 1339 (1958). doi:10.1021/ja01539a017

29. S. Zhu, Z. Liu, L. Hu, Y. Yuan, G. Xu, Turn-on fluorescence sensor based on single-walled-carbon-nanohorn–peptide complex for the detection of thrombin. Chem. Eur. J. **18**, 16556–16561 (2012). doi:10.1002/chem.201201468
30. G. Pagona, N. Tagmatarchis, J. Fan, M. Yudasaka, S. Iijima, Cone-end functionalization of carbon nanohorns. Chem. Mater. **18**, 3918–3920 (2006). doi:10.1021/cm0604864
31. C. Cioffi, S. Campidelli, C. Sooambar, M. Marcaccio, G. Marcolongo, M. Meneghetti, D. Paolucci, F. Paolucci, C. Ehli, G.M. Rahman, V. Sgobba, D.M. Guldi, M. Prato, Synthesis, characterization, and photoinduced electron transfer in functionalized single wall carbon nanohorns. J. Am. Chem. Soc. **129**, 3938–3945 (2007). doi:10.1021/ja068007
32. H. Isobe, T. Tanaka, R. Maeda, E. Noiri, N. Solin, M. Yudasaka, S. Iijima, E. Nakamura, Preparation, purification, characterization, and cytotoxicity assessment of water-soluble, transition-metal-free carbon nanotube aggregates. Angew. Chem. Int. Ed. **45**, 6676–6680 (2006). doi:10.1002/ange.200601718
33. C. Cioffi, S. Campidelli, F.G. Brunetti, M. Meneghetti, M. Prato, Functionalisation of carbon nanohorns, ChemComm 2129–2131 (2006). doi:10.1039/B601176D
34. N. Tagmatarchis, A. Maigne, M. Yudasaka, S. Iijima, Functionalization of carbon nanohorns with azomethine ylides: towards solubility enhancement and electron-transfer processes. Small **2**, 490–494 (2006). doi:10.1002/smll.200500393
35. T. Murakami, J. Fan, M. Yudasaka, S. Iijima, K. Shiba, Solubilization of single-wall carbon nanohorns using a PEG—doxorubicin conjugate. Mol. Pharm. **3**, 407–414 (2006). doi:10.1021/mp060027a
36. S. Matsumura, S. Sato, M. Yudasaka, A. Tomida, T. Tsuruo, S. Iijima, K. Shiba, Prevention of carbon nanohorn agglomeration using a conjugate composed of comb-shaped polyethylene glycol and a peptide aptamer. Mol. Pharm. **6**, 441–447 (2009). doi:10.1021/mp800141v
37. J. Xu, S. Iijima, M. Yudasaka, Appropriate PEG compounds for dispersion of single wall carbon nanohorns in salted aqueous solution. Appl. Phys. A **99**, 15–21 (2010). doi:10.1007/s00339-010-5582-7
38. M. Yang, M. Wada, M. Zhang, K. Kostarelos, R. Yuge, S. Iijima, M. Masuda, M. Yudasaka, A high poly(ethylene glycol) density on graphene nanomaterials reduces the detachment of lipid–poly(ethylene glycol) and macrophage uptake. Acta Biomater. **9**, 4744–4753 (2013). doi:10.1016/j.actbio.2012.09.012
39. M. Zhang, M.T. Murakami, K. Ajima, K. Tsuchida, O. Ito, S. Iijima, M. Yudasaka, Fabrication of ZnPc/protein nanohorns for double photodynamic and hyperthermic cancer phototherapy. Proc. Natl. Acad. Sci. U.S.A. **105**, 14773–14778 (2008). doi:10.1073/pnas.0801349105
40. E. Miyakoa, T. Deguchi, Y. Nakajima, M. Yudasaka, Y. Hagihara, M. Horie, M. Shichiri, Y. Higuchi, F. Yamashita, M. Hashida, Y. Shigeri, Y. Yoshida, S. Iijima, Photothermic regulation of gene expression triggered by laser-induced carbon nanohorns. Proc. Natl. Acad. Sci. USA, **109**, 7523–7528 (2012). doi:10.1073/pnas.1204391109
41. J.R. Whitney, S. Sarkar, J. Zhang, T. Do, T. Young, M.K. Manson, T. Campbell, A. Puretzky, C. Rouleau, K. More, D. Geohegan, C. Rylander, H. Dorn, M.N. Rylander, Single-walled carbon nanohorns as photothermal cancer agents. Lasers Surg. Med. **43**, 43–51 (2011). doi:10.1002/lsm.21025
42. E. Miyako, H. Nagata, K. Hirano, Y. Makita, K. Nakayama, T. Hirotsu, Near-infrared laser-triggered carbon nanohorns for selective elimination of microbes. Nanotechnology **18**, 475103 (2007). doi:10.1088/0957-4484/18/47/475103
43. E. Miyako, H. Nagata, K. Hirano, K. Sakamoto, Y. Makita, K. Nakayama, T. Hirotsu, Photoinduced antiviral carbon nanohorns. Nanotechnology **19**, 075106 (2008). doi:10.1088/0957-4484/19/7/075106
44. E. Miyako, C. Hosokawa, M. Kojima, M. Yudasaka, R. Funahashi, I. Oishi, Y. Hagihara, M. Shichiri, M. Takashima, K. Nishio, Y. Yoshida, A photo-thermal-electrical convertor based on carbon nanotubes for bioelectronic applications. Angew. Chem. Int. Ed. **51**, 2266–12270 (2011). doi:10.1002/ange.201106136

45. E. Miyako, H. Nagata, H. Hirano, T. Hirotsu, Carbon nanotube–polymer composite for light-driven microthermal control. Angew. Chem. Int. Ed. Engl. **47**, 3610–3613 (2008). doi:10.1002/anie.200800296
46. S. Chechetka, B. Pichon, M. Zhang, M. Yudasaka, S. Begin-Colin, A. Bianco, E. Miyako, Multifunctional carbon nanohorn complexes for cancer treatment. Chem. Asian J. **10**, 160–165 (2015). doi:10.1002/asia.201403059
47. T. Murakami, K. Ajima, J. Miyawaki, M. Yudasaka, S. Iijima, K. Shiba, Drug-loaded carbon nanohorns: adsorption and release of dexamethasone in vitro. Mol. Pharm. **1**, 399–405 (2004). doi:10.1021/mp049928e
48. K. Ajima, T. Murakami A. Maigne, K. Shiba, S. Iijima, Carbon nanohorns as anticancer drug carriers. Mol. Pharm. 2:475–80 (2005). doi:10.1021/mp0500566
49. K. Ajima, A. Maigné, M. Yudasaka, Sumio Iijima, Optimum Hole-opening condition for cisplatin incorporation in single-wall carbon nanohorns and its release. J. Phys. Chem. B **110**, 19097–19099 (2006). doi:10.1021/jp064915x
50. K. Ajima, T. Murakami, Y. Mizoguchi, K. Tsuchida, T. Ichihashi, S. Iijima, M. Yudasaka, Enhancement of in vivo anticancer effects of cisplatin by incorporation inside single-wall carbon nanohorns. ACS Nano **2**, 2057–2064 (2008). doi:10.1021/nn800395t
51. T. Murakami, H. Sawada, G. Tamura, M. Yudasaka, S. Iijima, K. Tsuchida, Water-dispersed single-wall carbon nanohorns as drug carriers for local cancer chemotherapy. Nanomed. Lond. **3**, 453–463 (2008). doi:10.2217/17435889.3.4.453
52. J. Xu, M. Yudasaka, S. Kouraba, M. Sekido, Y. Yamamoto, S. Iijima, Single wall carbon nanohorn as a drug carrier for controlled release. Chem. Phys. Lett. **461**, 189–192 (2008). doi:10.1016/j.cplett.2008.06.077
53. K. Tsuchida, T. Murakami, Recent advances in inorganic nanoparticle-based drug delivery systems. Mini Rev. Med. Chem. **8**, 175–183 (2008). doi:10.2174/138955708783498078
54. M. Nakamura, Y. Tahara, Y. Ikehara, T. Murakami, K. Tsuchida, S. Iijima, I. Waga, M. Yudasaka, Single-walled carbon nanohorns as drug carriers: adsorption of prednisolone and anti-inflammatory effects on arthritis. Nanotechnology **22**, 465102 (2011). doi:10.1088/0957-4484/22/46/465102
55. A.S.D. Sandanayaka, O. Ito, M. Zhang, K. Ajima, S. Iijima, M. Yudasaka, T. Murakami, K. Tsuchida, Photoinduced electron transfer in zinc phthalocyanine loaded on single-walled carbon nanohorns in aqueous solution. Adv. Mater. **21**, 4366–4371 (2009). doi:10.1002/adma.200901256
56. E. Miyako, J. Russier, M. Mauro, C. Cebrian, H. Yawo, C. Ménard-Moyon, J. Hutchison, M. Yudasaka, S. Iijima, L. De Cola, A. Bianco, Photofunctional nanomodulators for bioexcitation. Angew. Chem. Int. Ed. **53**, 13121–13125 (2014). doi:10.1002/annie.201407169
57. M. Mitsunaga, M. Ogawa, N. Kosaka, L. Rosenblum, P. Choyke, H. Kobayashi, Cancer cell–selective in vivo near infrared photoimmunotherapy targeting specific membrane molecules. Nat. Med. **17**, 1685–1691 (2011). doi:10.1038/nm.2554
58. X. Peng, D. Draney, W. Volcheck, G. Bashford, D. Lamb, D. Grone, Y. Zhang, C. Johnson, Phthalocyanine dye as an extremely photostable and highly fluorescent near-infrared labeling reagent. Proc. SPIE Int. Soc. Opt. Eng. **6097**, 113–124 (2006). doi:10.1117/12.669173
59. M. Ohkita, S. Saito, T. Imagawa, K. Takahashi, M. Tominaga, T. Ohta, Molecular cloning and functional characterization of xenopus tropicalis frog transient receptor potential vanilloid 1 reveal its functional evolution for heat, acid, and capsaicin sensitivities in terrestrial vertebrates. J. Biol. Chem. **287**, 2388–2397 (2012). doi:10.1074/jbc.M111.305698
60. R. Weissleder, A clearer vision for in vivo imaging. Nat. Biotechnol. **19**, 316–317 (2001). doi:10.1038/86684
61. X. Liu, L. Shi, W. Niu, H. Li, S. Han, J. Chen, G. Xu, Amperometric glucose biosensor based on single-walled carbon nanohorns. Biosens. Bioelectron. **23**, 1887–1890 (2008). doi:10.1016/j.bios.2008.07.001

62. L. Shi, X. Liu, W. Niu, H. Li, S. Han, J. Chen, G. Xu, Hydrogen peroxide biosensor based on direct electrochemistry of soybean peroxidase immobilized on single-walled carbon nanohorn modified electrode. Biosens. Bioelectron. **24**(2009), 1159–1163 (2009)
63. X. Liu, H. Li, F. Wanga, S. Zhu, Y. Wang, G. Xu, Functionalized single-walled carbon nanohorns for electrochemical biosensing. Biosens. Bioelectron. **25**, 2194–2199 (2010). doi:10.1016/j.bios.2010.02.027
64. J. Zhang, J. Lei, C. Xu, L. Ding, H. Ju, Carbon nanohorn sensitized electrochemical immunosensor for rapid detection of microcystin-LR. Anal. Chem. **82**, 1117–1122 (2010). doi:10.1021/ac902914r
65. I. Ojeda, B. Garcinuñ, M. Moreno-Guzman, A. Gonzalez-Cortes, M. Yudasaka, S. Iijima, F. Langa, P. Yanez-Sedeno, J. Pingarron, Carbon nanohorns as a scaffold for the construction of disposable electrochemical immunosensing platforms. Application to the determination of fibrinogen in human plasma and urine. Anal. Chem. **86**, 7749–7756 (2014). doi:10.1021/ac501681n
66. F. Yang, J. Han, Y. Zhuo, Z. Yang, Y. Chai, R. Yuan, Highly sensitive impedimetric immunosensor based on single-walled carbon nanohorns as labels and bienzyme biocatalyzed precipitation as enhancer for cancer biomarker detection. Biosens. Bioelectron. **55**, 360–365 (2014). doi:10.1016/j.bios.2013.12.040
67. WHO, *Guidelines for drinking-water quality, Addendum to Volume 2, Health Criteria and Other Supporting Information* (World Health Organization, Geneva, Switzerland, 1998)
68. J. Miyawaki, M. Yudasaka, T. Azami, Y Kubo, S. Iijima, Toxicity of single-walled carbon nanohorns, ACS Nano, **2**(2), 213–226 (2008). doi:10.1021/nn700185t
69. Y. Tahara1, J. Miyawaki,, M. Zhang, M. Yang, I. Waga, S. Iijima, H. Irie, M. Yudasaka, Histological assessments for toxicity and functionalization-dependent biodistribution of carbon nanohorns. Nanotechnology **22**, 265106, 8 (2011). doi:10.1088/0957-4484/22/26/265106
70. M. Zhang, T. Yamaguchi, S. Iijima, M. Yudasaka, Size-dependent biodistribution of carbon nanohorns in vivo, Nanomedicine. NBM **9**, 657–664 (2013). doi:10.1016/j.nano.2012.11.011
71. Y. Tahara, M. Nakamura, M. Yang, M. Zhang, S. Iijima, M. Yudasaka, Lysosomal membrane destabilization induced by high accumulation of single-walled carbon nanohorns in murine macrophage RAW 264.7. Biomaterials **33**, 2762–2769 (2012). doi:10.1016/j.biomaterials.2011.12.023
72. M. Yang, M. Zhang, Y. Tahara, S. Chechetka, E. Miyako, S. Iijima, M. Yudasaka, Lysosomal membrane permeabilization: Carbon nanohorn-induced reactive oxygen species generation and toxicity by this neglected mechanism. Toxicol. Appl. Pharmacol. **280**, 117–126 (2014). doi:10.1016/j.taap.2014.07.022
73. A. Hashimoto, H. Yorimitsu, K. Ajima, K. Suenaga, H. Isobe, J. Miyawaki, M. Yudasaka, S. Iijima, E. Nakamura, Selective deposition of a gadolinium(III) cluster in a hole opening of single-wall carbon nanohorn Proc. Natl. Acad. Sci. U.S.A. **101**, 8527–8530 (2004). doi:10.1073/pnas.0400596101
74. J. Miyawaki, M. Yudasaka, H. Imai, H. Yorimitsu, H. Isobe, E. Nakamura, S. Iijima, Synthesis of ultrafine Gd2O3 nanoparticles inside single-wall carbon nanohorns. J. Phys. Chem. B **110**, 5179–5181 (2006). doi:10.1021/jp0607622
75. R. Yuge, R. Ichihashi, J. Miyawaki, T. Yoshitake, S. Iijima, M. Yudasaka, Hidden caves in an aggregate of single-wall carbon nanohorns found by using Gd2O3 Probes. J. Phys. Chem. C **113**, 2741–2744 (2009)
76. J. Miyawaki, S. Matsumura, R. Yuge, T. Murakami, S. Sato, A. Tomida, T. Tsuruo, T. Ichihashi, T. Fujinami, H. Irie, K. Tsuchida, S. Iijima, K. Shiba, M. Yudasaka, Biodistribution and ultrastructural localization of single-walled carbon nanohorns determined in vivo with embedded Gd2O3 labels. ACS Nano **3**, 1399–1406 (2009). doi:10.1021/nn9004846
77. M. Zhang, Y. Tahara, M. Yang, X. Zhou, S. Iijima, M. Yudasaka, Quantification of whole body and excreted carbon nanohorns intravenously injected into mice. Advanced Healthcare Materials **3**, 239–244 (2013). doi:10.1002/adhm.201300192

78. H. Irie, W. Mori, Long term effects of thorium dioxide (Thorotrast) administration on heman liver. Acta Pathol. Jpn. **34**, 221–228 (1984). doi:10.1111/j.1440-1827.1984.tb07551.x
79. M. Yamamoto, K. Kato, Y. Ikada, Ultrastructure of the interface between cultured osteoblasts and surface modified polymer substrates. J. Biomed. Mater. Res. **37**, 29–36 (1997). doi:10.1002/(SICI)1097-4636(199710)37:1<29:AID-JBM4>3.0.CO;2-L
80. A.E. Porter, M. Gass, K. Muller, J.N. Skepper, P.A. Midgley, M. Welland, Direct imaging of single-walled carbon nanotubes in cells. Nat. Nanotechnol. **2**, 713–717 (2007). doi:10.1038/nnano.2007.347
81. C. Thakaral, J.L. Abraham, Automated scanning electron microscopy and X-ray microanalysis for in-situ quantification of gadolinium deposits in skin. J. Electron Microsc. **56**, 181–187 (2007). doi:10.1093/jmicro/dfm020
82. B.L. Allen, P.D. Kichambare, P. Gou, I. Vlasova, A. Kapralov, N. Konduru, V.E. Kagan, A. Star, Biodegradation of single-walled carbon nanotubes through enzymatic catalysis. Nano Lett. **8**, 3899–3903 (2008). doi:10.1021/nl802315h
83. B.L. Allen, G.P. Kotchey, Y. Chen, N. Yanamala, J. Klein-Seetharaman, V.E. Kagan, A. Star, Mechanistic investigations of horseradish peroxidase-catalyzed degradation of single-walled carbon nanotubes. J. Am. Chem. Soc. **131**, 17194–17205 (2009). doi:10.1021/ja9083623
84. V. Kagan, N. Konduru, W. Feng, B. Allen, J. Conroy, Y. Volkov, I. Vlasova, N. Belikova, N. Yanamala, A. Kapralov, Y. Tyurina, J. Shi, E. Kisin, A. Murray, J. Franks, D. Stolz, P. Gou, J. Klein-Seetharaman, B. Fadeel, A. Star, A. Shvedova, Carbon nanotubes degraded by neutrophil myeloperoxidase induce less pulmonary inflammation. Nat. Nanotechnol. **5**, 354–359 (2010). doi:10.1038/nnano.2010.44
85. Y. Zhao, B. Allen, A. Star, Enzymatic degradation of multiwalled carbon nanotubes. J. Phys. Chem. A **115**, 9536–9544 (2011). doi:10.1021/jp112324d
86. G.P. Kotchey, Y. Zhao, V.E. Kagan, A. Star, Peroxidase-mediated biodegradation of carbon nanotubes in vitro and in vivo. Adv. Drug Delivery Rev. **65**, 1921–1932 (2013). doi:10.1016/j.addr.2013.07.007
87. G.P. Kotchey, S.A. Hasan, A. Kapralov, S. Ha, K. Kim, A. Shvedova, V.E. Kagan, A. Star, A natural vanishing act: the enzyme-catalyzed degradation of carbon nanomaterials. Acc. Chem. Res. **45**, 1770–1781 (2012). doi:10.1021/ar300106h
88. A. Shvedova, A. Kapralov, W. Feng, E. Kisin, A. Murray, R. Mercer, C. St Croix, M. Lang, S. Watkins, N. Konduru, B. Allen, J. Conroy, G. Kotchey, B. Mohamed, A. Meade, Y. Volkov, A. Star, B. Fadeel, V. Kagan, Impaired clearance and enhanced pulmonary inflammatory/fibrotic response to carbon nanotubes in myeloperoxidase-deficient mice. PLoS ONE **7**, e30923 (2012). doi:10.1371/journal.pone.0030923
89. A. Nunes, C. Bussy, L. Gherardini, M. Meneghetti, M.A. Herrero, A. Bianco, M. Prato, T. Pizzorusso, K. Al-Jamal, K. Kostarelos, In vivo degradation of functionalized carbon nanotubes after stereotactic administration in the brain cortex. Nanomed. Lond. **7**, 1485–1494 (2012). doi:10.2217/nnm.12.33
90. Y. Sato, A. Yokoyama, Y. Nodasaka, T. Kohgo, K. Motomiya, H. Matsumoto, E. Nakazawa, T. Numata, M. Zhang, M. Yudasaka, H. Hara, R. Araki, O. Tsukamoto, H. Saito, T. Kamino, F. Watari, K. Tohji, Long-term biopersistence of tangled oxidized carbon nanotubes inside and outside macrophages in rat subcutaneous tissue. Sci. Rep. **3**, 2516 (2013). doi:10.1038/srep0216
91. V.E. Kagan, A. Kapralov, C. St, S.C. Croix, E.R. Watkins, G.P. Kisin, K.Balasubramanian Kotchey, I. Vlasova, J. Yu, K. Kim, W. Seo, R.K. Mallampalli, A. Star, A. Shvedova, Lung macrophages "digest" carbon nanotubes using a superoxide/peroxynitrite oxidative pathway. ACS Nano **8**, 5610–5621 (2014). doi:10.1021/nn406484b
92. M. Zhang, M. Yang, C. Bussay, S. Iijima, K. Kostarelos, M. Yudasaka, Biodegradation of carbon nanohorns in macrophage cells. Nanoscale **7**, 2834–3840 (2015). doi:10.1039/c4nr06175f